Research Article

Integrated terahertz vortex beam emitter for rotating target detection

Jingya Xie,[a] Jun Qian,[a] Tengjiao Wang,[a] Linjie Zhou,[b,*] Xiaofei Zang,[a] Lin Chen,[a] Yiming Zhu,[a,*] and Songlin Zhuang[a]

[a]University of Shanghai for Science and Technology, Terahertz Technology Innovation Research Institute, Shanghai Key Laboratory of Modern Optical System, Shanghai, China
[b]Shanghai Jiao Tong University, State Key Laboratory of Advanced Optical Communication Systems and Networks, Department of Electronic Engineering, Shanghai, China

Abstract. We propose a terahertz (THz) vortex emitter that utilizes a high-resistance silicon resonator to generate vortex beams with various topological charges. Addressing the challenge of double circular polarization superposition resulting from the high refractive index contrast, we regulate the transverse spin state through a newly designed second-order grating partially etched on the waveguide's top side. The reflected wave can be received directly by a linearly polarized antenna, simplifying the process. Benefiting from the tuning feature, a joint detection method involving positive and negative topological charges identifies and detects rotational Doppler effects amid robust micro-Doppler interference signals. This emitter can be used for the rotational velocity measurement of an on-axis spinning object, achieving an impressive maximum speed error rate of ∼2%. This approach holds promise for the future development of THz vortex beam applications in radar target detection and countermeasure systems, given its low cost and potential for mass production.

1 Introduction

The translational Doppler effect is a well-known frequency shift of electromagnetic waves that originates from the relative motion between the source and detector, and it has proven valuable in various applications, such as radar, passive location systems, satellite positioning, and navigation.[1–5] However, one limitation of traditional radar detection arises when the velocity vector of the target is perpendicular to the wave vector, leading to a blind spot in the detection process due to the challenge of extracting this particular motion component from the echo signal. To overcome this limitation, a new radar concept and system are required. One approach is by utilizing vortex electromagnetic waves carrying orbital angular momentum (OAM).[6] The vortex electromagnetic waves possess a helical phase structure described by $\exp(il_{TC}\varphi)$, where l_{TC} is an integer and φ is the azimuthal coordinate.[7] Specifically, when vortex electromagnetic waves are incident on a rotating target plane, they exhibit a phenomenon similar to the translational Doppler shift, known as the rotational Doppler effect, owing to the angle between the optical momentum and the central axis of the beam. The application of rotational Doppler detection in optics provides numerous advantages, including high resolution, strong anti-interference capability, and excellent collimation, rendering it highly suitable for low-altitude and precision detection scenarios.[8–13] In the realm of radio frequencies, this technique offers wide beam coverage, efficient penetration, and resilience against atmospheric and weather-related disturbances, making it an ideal choice for large-scale target detection applications even under all-weather conditions.[14–16] Terahertz (THz) waves, given their balanced characteristics encompassing penetration, collimation, resolution, and anti-interference capacity, represent a promising and novel avenue for the extraction and recognition of radar target features.

*Address all correspondence to Linjie Zhou, ljzhou@sjtu.edu.cn; Yiming Zhu, ymzhu@usst.edu.cn

Although numerous methods have been explored for generating vortex beams in the THz band,[17–23] current research mainly focuses on characterizing the OAM electric field, while their application in detection systems is still impeded by challenges, including low efficiency, instability issues arising from the requirement for high-precision alignment, and the utilization of bulky optical elements. A detailed comparison of the technologies used to generate THz vortex beams is provided in Table S1 in the Supplementary Material and Note 1 in the Supplementary Material. Moreover, it is crucial to note that in the THz band, a significant micro-Doppler effect occurs. The micro-Doppler effect is a phenomenon in which slight vibrations, rotations, or other motions of specific parts of an object generate modulation in a reflected signal.[24–26] This effect manifests sidelobes or spectral broadening in the spectral domain. While conventional radar systems operating in lower frequency bands typically experience negligible micro-Doppler effects, THz radar operating in higher frequency bands faces significant micro-Doppler effects.[27] Therefore, it is crucial to accurately differentiate the rotational Doppler frequency shift from the micro-Doppler frequency shifts in practical THz rotational detection applications. One possible solution is to utilize multiple OAM modes in combination for detection, thereby increasing the feature dimension of the rotational Doppler signal. However, as highlighted in Table S1 in the Supplementary Material, the tunability of conventional THz vortex beam generation methods is limited. Although mechanical tuning can change the topological charge, its low stability and accuracy preclude optimal utilization. Another approach involves the dynamic modulation of photo-generated carriers in silicon, but it requires expensive spatial light modulators that have a low laser damage threshold. Hence, further investigation is imperative to explore more practical and tunable THz vortex generators, as well as corresponding detection schemes for the rotational Doppler effect. This will fully exploit the distinctive attributes of THz vortex beams in the realm of rotating detection technology.

In this study, we present what we believe is a novel approach for the joint detection of rotational velocity using vortex beams with positive and negative topological charges, facilitated by an integrated THz vortex beam emitter. Our design involves the manipulation of the frequency to access different resonances within the cavity, thereby enabling the generation of vortex beams with ±1 topological charges. These vortex beams are subsequently illuminated onto a rotating object, and the resulting echo spectra from the two beams are carefully analyzed and compared. Through effective identification and detection of the rotational Doppler effect within the frequency spectrum, we can accurately quantify the rotational velocity of the object under investigation. To ensure high compactness and stability, the device is fabricated using a high-resistance silicon wafer, aligning with previous studies.[28–31]

Our device builds upon the foundation of a whispering gallery mode (WGM) resonator-based optical vortex emitter.[32] However, a conventional emitter of this kind generates a cylindrical vector vortex (CVV) beam that features cylindrically symmetric states of polarization and helical phase fronts.[33] The beam is composed of two circularly polarized lights with different topological charges, yielding a complex polarization state. Such complexity in polarization is unsuitable for THz reception detection. In THz applications, scalar antennas, primarily linearly polarized ones, are commonly employed as receiving antennas, rendering the vector beam insufficient for

potential detection purposes. Therefore, achieving scalar THz vortex beams using the mentioned emitter becomes crucial. In response to this challenge, we conduct a comprehensive analysis that takes into account the spin–orbit interaction effect, where transverse spin is defined as the spin angular momentum in evanescent waves with its axis perpendicular to the direction of light propagation.[33] We propose a novel second-order grating to regulate the transverse spin. The second-order grating is named as such because its second-order diffraction reflects light back into the contra-propagating waveguide mode, whereas the first-order diffraction allows light to couple out of the waveguide at a 90-deg angle, resulting in the generation of a surface-normal propagating field. Our method involves the partial etching of the grating on the top side of the ring waveguide within the THz vortex beam emitter, effectively suppressing one of the circular polarizations and enabling the creation of a single circularly polarized vortex beam. Utilizing the rotational Doppler effect, we have successfully employed our THz scalar vortex beam emitter for the detection of angular velocity in rotating targets. By coupling a linearly polarized metal waveguide with our device, we are able to excite a scalar circularly-polarized vortex beam. This configuration allows for direct reception of the echo reflected by a rotating target using a linearly polarized antenna, thereby significantly simplifying the detection process. By manipulating the frequency to access different resonances within the device, we can generate a range of vortex beams with distinct topological charges. In this particular investigation, we focus on vortex beams possessing ±1 topological charges to investigate the rotational Doppler frequency shift phenomenon. Through a meticulous comparison of the two detection spectra, we can effectively discern the rotational Doppler frequency shift. By extracting the position of this frequency shift, we can accurately calculate the rotational velocity of the target object. To the best of our knowledge, this study represents the first demonstration of an integrated THz vortex beam emitter specifically designed for the detection of rotating targets.

2 Results and Discussion

Figure 1 provides an illustrative representation of the designed chip-scale THz vortex beam emitter on a silicon platform. In this configuration, a quasi-transverse-electric (quasi-TE) mode wave (the transverse dominant component of the electric field is in the y direction) is coupled from the bus waveguide into the ring resonator, thereby exciting the WGMs. The ring utilized in our experiment was fabricated using ridge-type silicon waveguides that were 500 μm wide and 340 μm high and placed over a 130 μm slab. The radius of the ring resonator is 6900 μm, while 72 grating elements are positioned along the top and inner sides of the ring waveguide, each having a size of 350 μm × 350 μm × 60 μm ($a \times b \times c$). The grating period Λ is ~602 μm, with a 100 μm gap separating the bus waveguide from the ring resonator. The ridge height of the bus waveguide is 400 μm. To attain critical coupling and maximize emission efficiency, we reduced the width of the bus waveguide to 400 μm. The fabricated device's optical microscope images are shown in Fig. 1(b), while additional details of the fabrication process are available in Sec. 4. The device generates a single left-hand circular polarization (LHCP) OAM beam that results in emitted vortex beams featuring the desired singularities and helical phase observed in either the x or y component of the electric field, which can be directly received via a linearly polarized
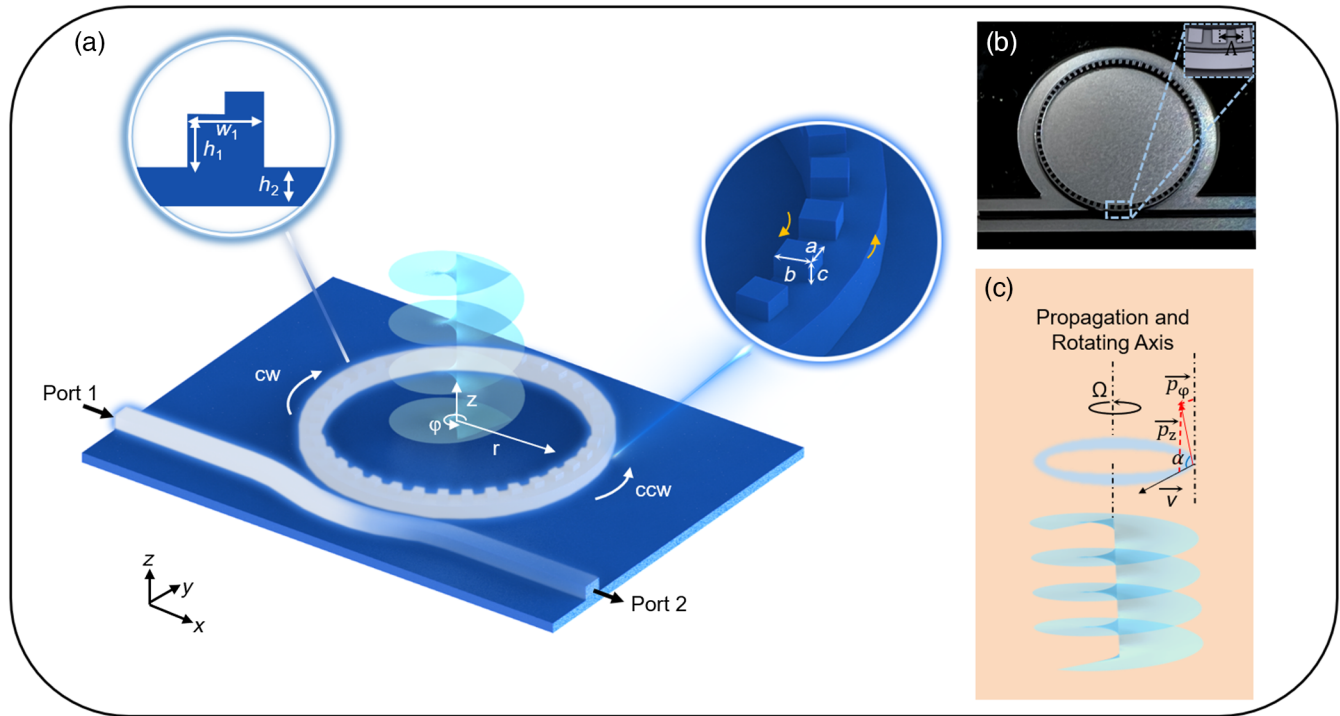
Fig. 1 Illustration of the concepts. (a) Schematic of the designed integrated THz vortex beam emitter. The insets depict the geometry of the waveguide cross section and grating scatterers, which are all cuboid in shape. (b) Optical microscope images of the fabricated device. The inset is a zoomed-in view of the grating scatterers and the coupling section between the bus waveguide and the resonator. (c) Schematic of rotational Doppler effect. A tiny scatterer from a rotating body is taken out to analyze the relationship between the Poynting vector and the scatterer velocity on the condition of coaxial incidence. $\vec{p}_\varphi$ and $\vec{p}_z$ are the angular and the propagation components, respectively.

THz antenna. The basic principle of using the rotational Doppler effect to detect the rotation speed of objects is shown in Fig. 1(c). As the Poynting vector characterizing the energy flow density does not align with the vortex beam's propagation axis, a momentum component emerges in the transverse plane $\vec{p}_\varphi$. Consequently, there will be a Doppler frequency shift of the echo signal from the rotating object.

In the high-index waveguide, a local longitudinal electric component ($\mathbf{E}_\varphi$) exists in the evanescent waves, which is quadrature-phased with respect to the radial component ($\mathbf{E}_r$). Therefore, the evanescent field possesses a "transverse" spin axis in the z direction, which is orthogonal to the local propagation direction ($+\varphi$ or $-\varphi$) of the WGM. To generate diffracted first-order light from the evanescent fields of the WGMs, a second-order grating strategically placed in the inner sidewall evanescent region of the waveguide is used.[32,33] This configuration enables the generation of a vortex beam carrying OAM and propagating perpendicular to the resonator plane. However, employing this approach often leads to the generation of a CVV beam characterized by cylindrically symmetric polarization and intensity distributions. Assuming that the light is coupled from the left port (Port 1) and excites the counterclockwise (CCW) propagating WGM, the resulting CVV beam comprises LHCP and right-hand circular polarization (RHCP) vortices. These vortices possess topological charges of $l_{TC} - 1$ and $l_{TC} + 1$, respectively.[32] The topological charge l_{TC} satisfies the selection rule of $l_{TC} = \pm(p - q)$, where p is the WGM order in the ring and q is the number of grating

elements around the resonator. By simply adjusting the input wavelength to match different ring cavity resonances, the topological charge can be tuned accordingly. It is important to note that the specific OAM component carried by the CVV beam is determined by the transverse spin state of the WGM evanescent wave, owing to the spin–orbit interaction effect. In essence, the manipulation of transverse spin in evanescent waves allows for the generation of vector vortex beams with varying polarization states (see Note 2 in the Supplementary Material for details). The ability to control the transverse spin is made possible by the design of a grating with a square section and the careful adjustment of the waveguide width.[33] It is crucial to acknowledge that the transverse spin state in the evanescent wave of the waveguide is heavily influenced by the ratio of longitudinal and transverse field components, which, in turn, is strongly influenced by the refractive index contrast of the waveguide. Consequently, achieving an approximation of the transverse spin to ± 1 in waveguides with high refractive index contrast presents a significant challenge when aiming to generate a single LHCP or RHCP light using this ring-based vortex beam emitter. This challenge is particularly profound in THz silicon waveguides, as conventional low-loss integrated THz waveguides employ high-resistance silicon as the core layer and air as the cladding layer. Their refractive index contrast surpasses that of silicon-on-insulator and silicon nitride waveguides with SiO_2 cladding in the optical domain. A higher index contrast amplifies the magnitude of the ratio $i\mathbf{E}_\varphi/\mathbf{E}_r$ near the sidewalls of the waveguide, particularly for the TE mode

(refer to Note 3 in the Supplementary Material for elucidation). Although the ratio of the two electric components of the radiation field κ is also influenced by the scatterer modulation on the electric component's strength, the extent to which κ can be adjusted by varying the size of the grating scatterers is limited. This limitation arises from the limited evanescent field depths, which are characterized by the $1/e$ exponential decay distance and typically span tens of micrometers. Consequently, approximating the transverse spin as ± 1 poses a considerable challenge.

According to the information provided in Note 3 in the Supplementary Material, it is evident that even in scenarios characterized by high refractive index contrast, weak electric fields $\mathbf{E}_{\varphi}$ manifest at the top and bottom of the waveguide for the TE mode. To maintain a low magnitude of the $i\mathbf{E}_{\varphi}/\mathbf{E}_r$ ratio, a well-designed grating can be positioned. Subwavelength grating scatterers can be precisely etched on the top of the ring waveguide to achieve this purpose. It is important to note that the transverse spin on the inner and outer sidewalls of the waveguide exhibits opposite spin directions. Enveloping the whole waveguide with the grating scatterers results in the generation of dual circularly polarized light. Consequently, for optimal performance, the top grating scatterers should only be etched on one side, as shown in Fig. 1. Notably, at the waveguide's upper section, the $i\mathbf{E}_{\varphi}/\mathbf{E}_r$ ratio is small, and the size of the grating associated with the evanescent field corresponds to the etching depth c. As a result, the in-plane parameters a and b are not limited by the evanescent field and can be adjusted over a broader range by modulating the scatterers' influence on the φ and r directions. There exists notable variability in the regulation range of transverse spin, which has a direct impact on the final radiated vortex beam composition resulting from spin-orbital angular momentum coupling. As a result, the proposed grating, which is partially etched on the top, offers the advantage of being easier to maintain a single transverse spin state in comparison to conventional gratings that are etched on the waveguide's sidewall. We systematically optimize and fix the etching depth of the grating while adjusting its transverse size to meet the ± 1 transverse spin requirement. Furthermore, the scattering within the desired frequency range is achieved by optimizing the grating period.

The transmission spectrum of the device was initially recorded for the TE polarization using the method detailed in our prior work.[30,31] The device was measured using a THz continuous-wave electronic system comprising an R&S ZNA26 vector network analyzer (VNA) and a collection of 140 to 220 GHz VNA extenders. The VNA extender and the device are connected by two WR-5.1 waveguides. A micromechanical positioner was utilized to carefully manage the position of the sample and the WR-5.1 waveguide. To generate the transmission spectral response, the frequency was swept from 176 to 189 GHz in 0.1 GHz increments. Each distinctive resonance observed in Fig. 2(a) corresponds to a distinct WGM resonance (p value). This attribute of the device leads to the observation of vortex beams with different topological charges at specific resonance frequencies. For instance, the frequency corresponding to a zero topological charge ($l_{TC} = 0$) is 180.78 GHz. At adjacent resonances to the zero topological charge position, two modes corresponding to $l_{TC} = \pm 1$ are created. At resonance frequencies of 177.04, 178.85, 182.61, and 184.44 GHz, the device exhibits l_{TC} values of -2, -1, 1, and 2, respectively, as indicated by the corresponding transmission spectrum. The free spectral range is ~ 1.85 GHz. The Q-factor values for the resonances corresponding to $l_{TC} = 1$ and -1 are 190 and 201, respectively.

The device's near-field experimental characterizations were conducted utilizing the setup depicted in Fig. 2(b). The excitation of the quasi-TE mode in the bus waveguide was achieved by launching a vertically polarized wave, which exhibited effective coupling from a WR-5.1 waveguide. Another WR-5.1 waveguide facilitated the connection of the near-field probe to a distinct VNA extender. Positioned at a distance of 8 mm, equivalent to ~ 5 times the wavelength at the central frequency, the linearly polarized probe efficiently collected x- and y-polarized THz waves while serving as the receiver. Step-by-step movement of the probe along the x and y directions facilitated the acquisition of the near-field's intensity and phase distributions, shown in Fig. 3. The scanning plane encompassed an area of 3.42 mm $\times$ 3.42 mm, effectively covering the primary radiation region of the device. Notably, both simulated and measured x-o-y planes displayed distinctive doughnut-shaped intensity

(a)

(b)
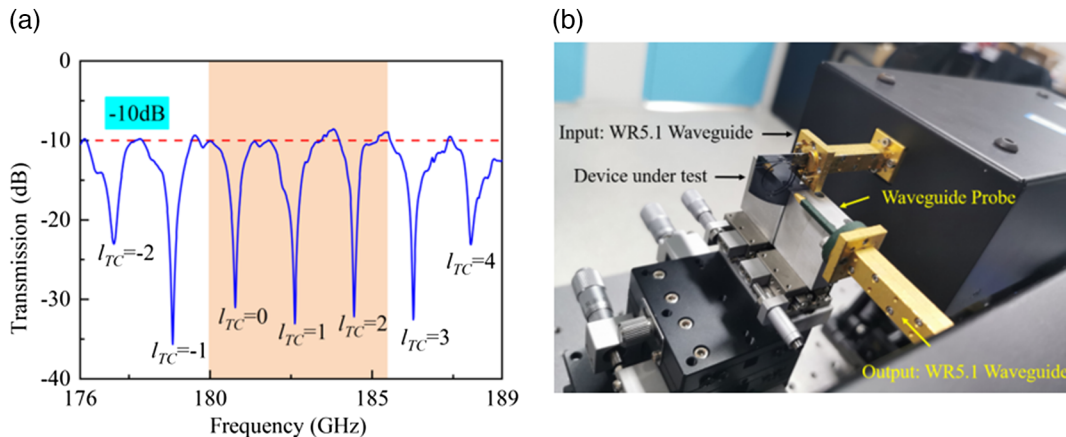
Fig. 2 (a) Measured transmission spectrum of the THz vortex emitter for the TE mode. Note that the black annotation indicates the topological charge l_{TC}. The orange region represents the frequency range used for near-field and rotational Doppler experiments. (b) Experimental setup for device near-field characterization.
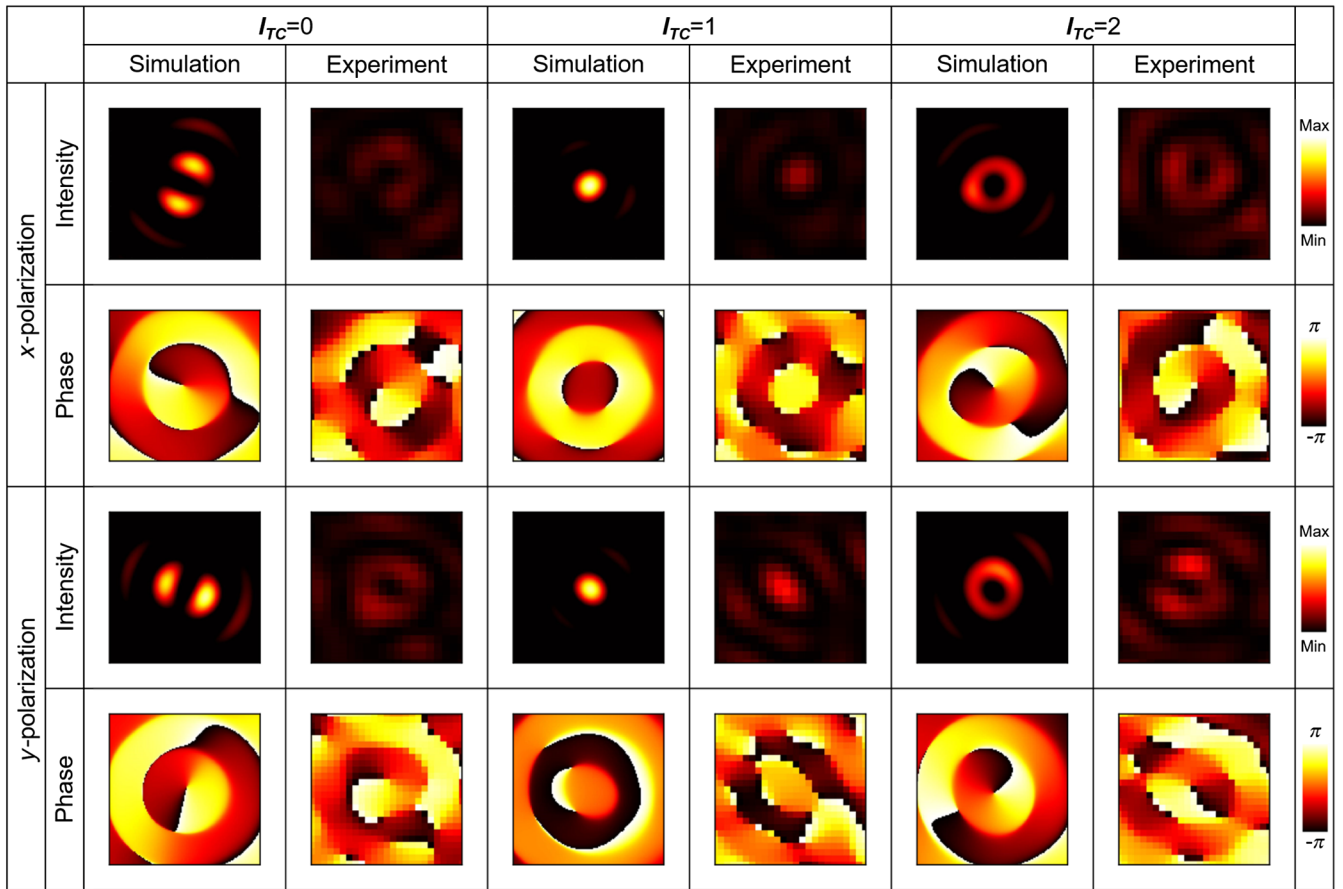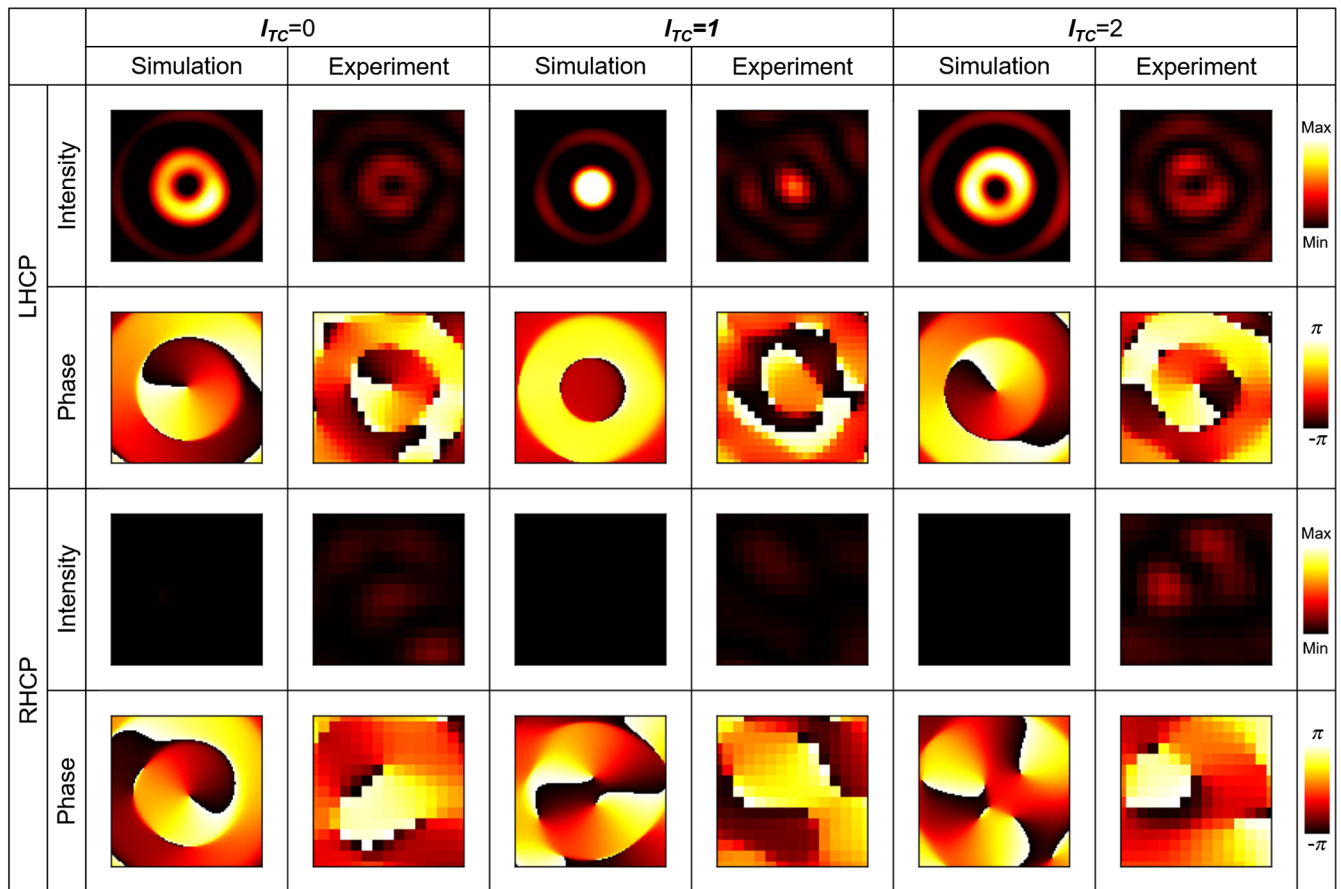
Fig. 3 Simulated and measured radiation cross-sectional field distributions of the x and y polarization components for our device with the corresponding l_{TC}. Note that $l_{TC} = p - q$ is the topological charge, where p is the azimuthal order of WGM, and q is the number of grating elements.

distributions, while the simulated and measured phase distributions exhibited helical twist patterns. Although slight variations in intensity and inhomogeneity were observed, the qualitative agreement between the measured intensity and phase distributions, as shown in Fig. 3, and the simulation results indicated the successful generation of vortex beams with OAM modes of $l = l_{TC} - 1$ (-1, 0, and 1). It was observed that obtaining an accurate helical phase was possible when receiving the beam with either x or y polarization. The experimental findings demonstrate that the implementation of a grating element etched on the waveguide's top surface greatly reduces one of the circularly polarized beams, particularly when l_{TC} is equal to 2. If a single scalar vortex beam is not well produced, a vortex beam with topological charges of ± 1 will have multiple vortex singularities in its x or y polarization electric field. Detailed simulation results are provided in Note 4 in the Supplementary Material.

To validate this principle, Fig. 4 shows the intensity and phase distributions of two orthogonal scalar vortices, LHCP and RHCP. These scalar vortices are generated by combining the amplitude and phase responses of two orthogonal linearly polarized waves. The intensity and phase distributions reveal that the emitted CVV beam can be expressed as a superposition of two orthogonal scalar vortices: an RHCP beam with a topological charge of $l_{TC} + 1$ and an LHCP beam with $l_{TC} - 1$. By examining the figures, it is evident that the scalar vortex beam is successfully generated. The power of the vortex electric field for LHCP is significantly higher than that of RHCP. The agreement between the measured and simulated results substantiates the proposed design and confirms the successful manipulation of the vortex component. Hence, the device is capable of emitting a single scalar vortex beam upward. For the LHCP beam, the OAM mode $l_{TC} - 1$ is -1, 0, 1 which corresponds to the phased change of x or y polarization in Fig. 3.

The utilization of the rotational Doppler effect for rotation speed measurement has garnered significant attention. However, the prevailing methods primarily rely on optical beams and microwaves, with limited exploration of THz vortex beams for this purpose, particularly in the context of integrated on-chip devices. Furthermore, the THz frequency band poses challenges in accurately identifying and detecting the rotational Doppler effect due to a prominent micro-Doppler effect. By harnessing the tuning capability of our device, we effectively detect and identify the rotational Doppler effect, thereby facilitating precise measurement of rotational velocity in the THz domain. The experimental configuration is shown in Fig. 5. We employed a Rohde & Schwarz signal generator (SMB100A) in conjunction with a broadband frequency multiplication chain to generate the THz wave in a WR-5.1 waveguide. Subsequently, the vortex beam is generated by coupling the THz wave into the bus waveguide of our device. The generated vortex beam is then collimated using an off-axis parabolic mirror with a focal length of 152.4 mm before being irradiated onto the surface of a

Fig. 4 Simulated and measured radiation cross-sectional field distributions of the LHCP and RHCP components for our device with the corresponding l_{TC}.
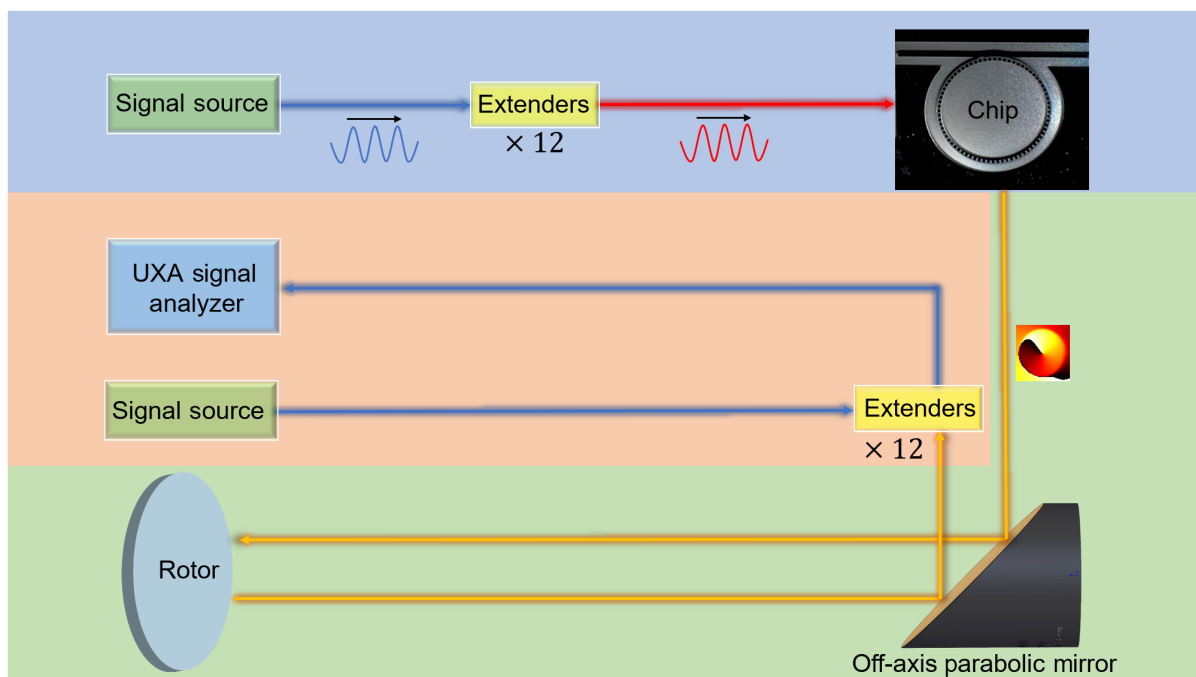
Fig. 5 Schematic diagram for experimental setup of rotation speed measurement of a spinning object using the vortex beam generated by the integrated THz chip.

rotating object. The rotor employed is an optical chopper without blades, ensuring precise control over the rotation speed. The distance between the source and the rotor is 26.7 cm. It is worth emphasizing that our detection method distinguishes itself from established techniques in the optical domain.[12]

This work introduces a novel method that obviates the requirement for half-wave plates or polarization beam splitters to process the output vortex beam. This constitutes a notable advantage, particularly in the THz frequency band, where optical components, such as diverse wave plates, may not be easily
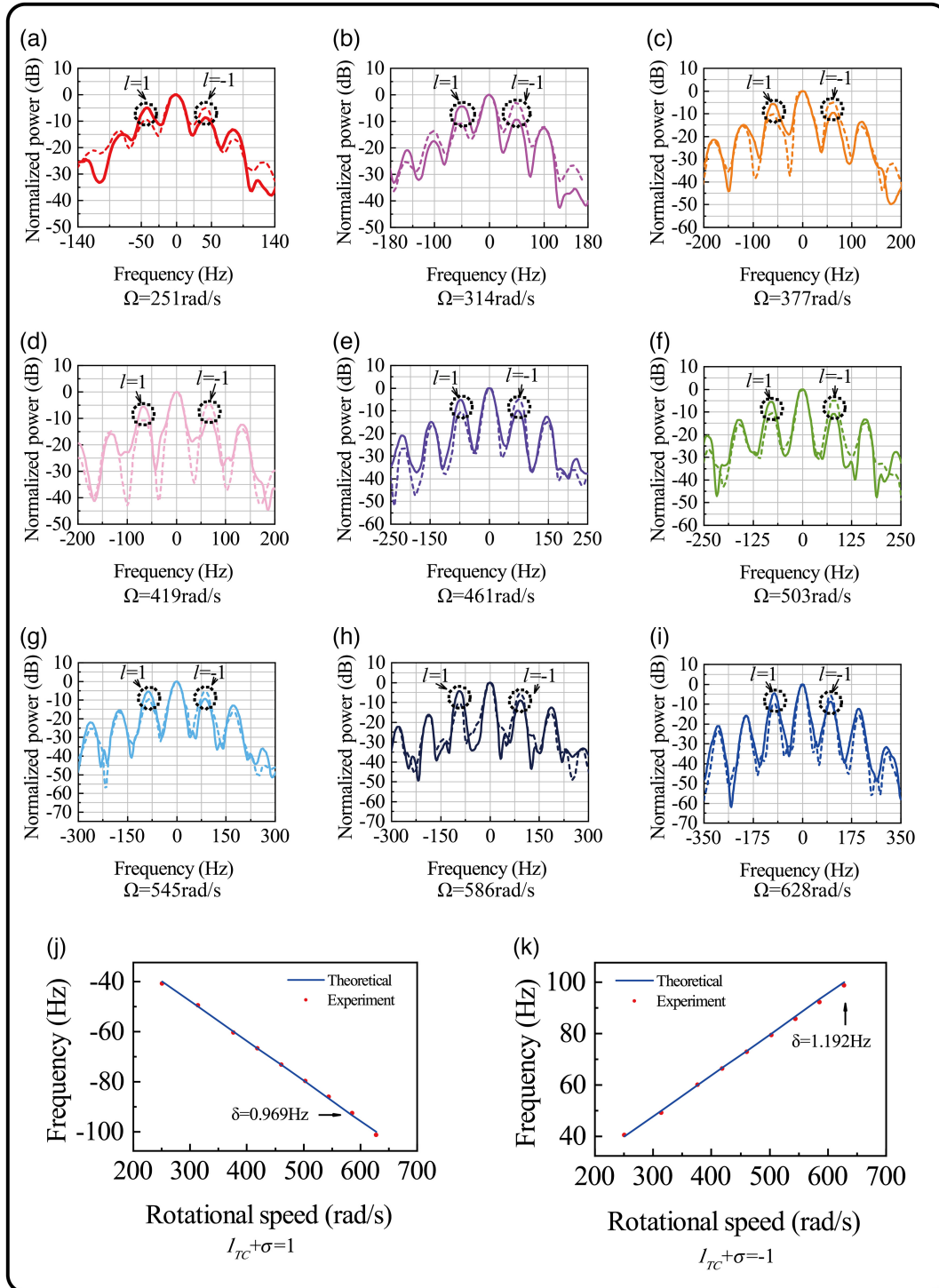
Fig. 6 Measurement results of rotating speed using vortex beam generated on-chip. (a)–(i) The observed power spectrum at the indicated rotational speed. (j) The measured results at different rotating speeds for OAM mode +1. (k) The measured results at different rotating speeds for OAM mode −1. For (j) and (k), the rotational speeds are from 251 to 628 rad/s. The red points are the measured data, and the solid blue lines are the theoretical values. Note that δ is the absolute error.

accessible. In addition, THz devices are generally costly, thereby underscoring the great practical and research significance of the direct detection approach adopted in this experiment. In contrast to optics, THz waves exhibit a greater degree of divergence, and obtaining the whole reflected wave to measure the rotational Doppler frequency shift is not possible. Therefore, the rotational Doppler frequency shift for the THz vortex beam is gained through the spectrum of the local backward wave. Upon illuminating a rotating object with an incident vortex beam, the reflected wave is collected directly using a linear polarization horn antenna. A spectrum analyzer extender driven by a sine wave local oscillator (Keysight, PSG E8257D) is leveraged to down-convert the THz electrical signal into a lower-frequency signal. Next, the intermediate frequency signal is measured using a frequency spectrum analyzer (Keysight, UXA N9040B) via a phase-stable coaxial cable in order to obtain the rotational Doppler frequency shift via spectrum analysis.

The helical phase front of the OAM carrying wave is represented by $\exp[-j(l_{TC} + \sigma)\varphi]$, where σ is equal to ± 1 for right- and left-handed circular polarizations and 0 for linear polarization. In the case of a helically phased beam incident at normal angles, the Poynting vector exhibits an azimuthal component at every position within the beam. Upon illuminating a rotating object along the transmission axis of the vortex beam, a rotational Doppler frequency shift Δf_r can be obtained from the reflected wave, akin to the translational Doppler frequency shift. This frequency shift can be expressed as[9]

$$\Delta f = (l_{TC} + \sigma) \cdot \Omega/2\pi, \qquad (1)$$

where Ω is the rotational velocity of the object. This principle forms the foundation for the detection of rotational speeds of objects. At every position within the beam, including the phase singularity point that coincides with the center of rotation, an identical modulation frequency is encountered. Consequently, by detecting the frequency shift between the reflected wave and the incident wave, it becomes possible to accurately measure the rotational velocity of the object.

Figures 6(a)–6(i) show the power spectra obtained from our rotational Doppler detection experiment. The dominant peak corresponds to the reflected wave in the absence of rotation (static configuration). We measured the local backward wave for nine different experimental scenarios, with angular velocities $\Omega = 251, 314, 377, 419, 461, 503, 545, 586,$ and 628 rad/s. By employing an LHCP vortex beam with a topological charge of $l_{TC} - 1 = \pm 1$, we observed rotational Doppler frequency shifts $\Delta f_- = -\Omega/2\pi$ and $\Delta f_+ = +\Omega/2\pi$, respectively. For instance, in Fig. 6(a), in addition to the main peak originating from the direct coupling effect, a secondary frequency peak is evident. Notably, this peak is detected at a frequency of -40.812 Hz for the topological charge $l_{TC} - 1(+1)$, and at $+40.812$ Hz for $l_{TC} - 1 (-1)$. The experimental results for various rotational speeds (251 to 628 rad/s) conform well to the theoretical predictions represented in Figs. 6(j) and 6(k). Figure 6(j) is associated with the topological charge $+1$, while Fig. 6(k) is related to the topological charge -1. The highest absolute error δ for topological charge $+1$ is 0.969 Hz, observed at a speed of 586 rad/s, while the maximum relative error for topological charge $+1$ is $\sim 2\%$, occurring at a speed of 251 rad/s. Similarly, the highest absolute error δ for topological charge -1 is 1.192 Hz at a speed of 628 rad/s, with the maximum

relative error for topological charge -1 being $\sim 2\%$, observed at a speed of 251 rad/s. The results reveal that the measured frequency shift increases linearly with the rotational speed and that the velocity measurement accuracy is high, which can be further enhanced via calibration. This work presents the first successful measurement of rotation speed using a THz vortex beam generated from an integrated chip.

It is important to highlight that the spectrum exhibits various peaks associated with micro-Doppler frequency shifts, overlapping with the rotating Doppler signal. Meanwhile, we also note that the micro-Doppler frequency shift peak with a larger frequency shift exhibits relatively lower power in the spectrum. The peaks within the micro-Doppler frequency effect spectrum, with frequency shifts of $\pm\Omega/2\pi$ and $\pm\Omega/\pi$, are considered as the primary peaks. Higher-order peaks may be disregarded. When the incident vortex beam possesses a topological charge of $l_{TC} - 1 = \pm 1$, the micro-Doppler frequency shift corresponding to the primary peak aligns with the rotational Doppler frequency shift. By comparing the positive and negative frequency shift peaks generated by the opposite sign of the topological charge, we can solely detect the rotational Doppler signal overlaid on the micro-Doppler signal. This joint detection method enables the effective identification of the rotational Doppler shift signal at $\Delta f_- = -\Omega/2\pi$ and $\Delta f_+ = +\Omega/2\pi$, as depicted by the black circle in Fig. 6. By utilizing the principle of the rotating Doppler effect, it is anticipated that a higher-order LHCP vortex beam, specifically designed for this purpose, can amplify the rotating Doppler shift by $l_{TC} - 1$. This amplification generates signals at further sideband locations with sufficient significance to surpass the micro-Doppler effect. Hence, to differentiate the rotational Doppler frequency shift from the micro-Doppler frequency shift more clearly, it is necessary to utilize a vortex beam with a larger topological charge as the detecting wave. Furthermore, the multiplication of the rotational Doppler frequency shift by the larger topological charge will also improve the detection of small rotating speeds. In our work, the vortex emitter is reliant on high-resistance silicon to achieve high excitation efficiency. When selecting materials other than silicon for the vortex emitter at THz frequencies, careful evaluation is required to achieve balanced performance, such as low loss, high refractive index, and ease of fabrication.

3 Conclusion

In summary, we have successfully developed and demonstrated an integrated vortex emitter operating in the THz frequency range. This silicon-integrated THz chip represents a remarkable achievement, as it enables the emission of vortex beams that can be utilized for rotational speed measurement. The key to this accomplishment lies in the design of a compact scalar LCHP/RCHP vortex emitter. This emitter allows for the tuning of topological charges and enables the direct detection of linear polarization electric field through a horn antenna. By implementing a novel second-order grating structure, partially etched on the waveguide's top side, we achieved a transverse spin close to ± 1, resulting in the generation of a single circularly polarized vortex component. Comprehensive numerical simulations and near-field measurements have been conducted to validate this approach and investigate the electric field and phase properties of the emitter. In the experiment, vortex beams with topological charges of ± 1 were employed to explore the rotational Doppler effect for measuring the rotational velocity of an object. The

experiment yielded a maximum rotational velocity error of ~2%. To further enhance the accuracy of the rotational speed measurement, the chip can be optimized by adjusting the grating parameters and the coupling strength of the bus waveguide and ring. This optimization strategy has the potential to enable the emission of a scalar vortex beam with a higher topological charge, leading to a more precise measurement of rotational velocity. These results highlight the promising potential of THz-integrated vortex beam chips in various applications, including the detection of propeller rotation in aircraft during stable flight conditions. Such technology holds significant practical implications across diverse industries and fields.

4 Appendix

4.1 Fabrication

The device was fabricated on a 10.16 cm intrinsic double-sided polished silicon wafer with a thickness of 530 μm and a resistivity of 20 k$\Omega \cdot$ cm. Initially, a 1.3 μm SiO$_2$ film was deposited on the silicon wafer using plasma-enhanced chemical vapor deposition techniques. Then, the grating patterns were transferred to the SiO$_2$ hard mask via reactive ion etching. Standard ultraviolet lithography and inductively coupled plasma etching were subsequently used to fabricate the device. A thick positive photoresist (AZ P4620) was spin-coated and patterned to form a thick photoresist mask. During the fabrication process, two etching procedures were executed on the silicon wafer. The primary etching formed the ridge-type waveguides for both the ring and bus waveguides, with an etching depth of 340 μm. The second etching generated the grating with a depth of 60 μm, utilizing the SiO$_2$ hard mask. Moreover, in the same process, the slab area was also etched to form a holder with a thickness of 130 μm. Finally, the fabricated wafer was diced into individual components for testing.

4.2 Numerical Simulation

The radiation cross-sectional field distributions of our devices and the modes of the dielectric waveguides are numerically calculated with a finite-difference time-domain method and a finite-difference eigenmode solver (Lumerical Solutions, Inc.), respectively.

Data Availability

The data that support the findings of this study are available from the corresponding author upon reasonable request.

Author Contributions

J.X. and Y.Z initiated the idea. J.Q. and T.W. conducted the numerical simulations. J.X., J.Q., and T.W. performed the measurements. J.X., J.Q., T.W., L.Z., X.Z., L.C., Y.Z., and S.Z. prepared the manuscript. All the authors discussed and analyzed the results.

Acknowledgments

References

1. S. J. Ostro, "Planetary radar astronomy," *Rev. Mod. Phys.* **65**(4), 1235 (1993).
2. Y. T. Chan and F. L. Jardine, "Target localization and tracking from Doppler-shift measurements," *IEEE J. Ocean. Eng.* **15**(3), 251–257 (1990).
3. J. N. J. Cafarelli, "Doppler frequency position fixing method," U.S. patent 2,968,034 (1961).
4. S. C. Jasper, "Method of Doppler searching in a digital GPS receiver," U.S. patent 4,701,934 (1987).
5. Y. D. Zhao et al., "Detection of moving targets based on Doppler spectrum analysis technique for passive coherent radar," *J. Rad.* **2**(2), 247–256 (2013).
6. Z. Y. Guo et al., "Research advances on the rotational Doppler effect of vortex electromagnetic waves," *J. Rad.* **10**(5), 725–739 (2021).
7. L. Allen et al., "Orbital angular momentum of light and the transformation of Laguerre-Gaussian laser modes," *Phys. Rev. A.* **45**(11), 8185–l8189 (1992).
8. N. Gerard, "Doppler effect induced by rotating lenses," *Opt. Commun.* **132**(1–2), 8–14 (1996).
9. M. P. J. Lavery et al., "Detection of a spinning object using light's orbital angular momentum," *Science* **341**(6145), 537–540 (2013).
10. H. Zhou et al., "Theoretical analysis and experimental verification on optical rotational Doppler effect," *Opt. Express* **24**(9), 10050–10056 (2016).
11. Y. W. Zhai et al., "Detection of angular acceleration based on optical rotational Doppler effect," *Opt. Express* **27**(11), 15518–15527 (2019).
12. Y. W. Zhai et al., "Remote detection of a rotator based on rotational Doppler effect," *Appl. Phys. Express* **13**(2), 022012 (2020).
13. S. Qiu et al., "Spinning object detection based on perfect optical vortex," *Opt. Lasers Eng.* **124**, 105842 (2020).
14. K. Liu et al., "Microwave imaging of spinning object using orbital angular momentum," *J. Appl. Phys.* **122**(12), 124903 (2017).
15. Z. Zhou et al., "Rotational Doppler resolution of spinning target detection based on OAM beams," *IEEE Sens. Lett.* **3**(3), 18509557 (2019).
16. C. Brousseau, K. Mahdjoubi, and O. Emile, "Measurement of the rotational sense and velocity of an object using OAM wave in the radio-frequency band," *Electron. Lett.* **55**(12), 709–711 (2019).
17. K. Miyamoto et al., "Direct observation of the topological charge of a terahertz vortex beam generated by a Tsurupica spiral phase plate," *Appl. Phys. Lett.* **104**(26), 261104 (2014).
18. X. F. Zang et al., "Metasurfaces for manipulating terahertz waves," *Light: Adv. Manuf.* **2**(2), 148–172 (2021).
19. J. W. He et al., "Generation and evolution of the terahertz vortex beam," *Opt. Express* **21**(17), 20230–20239 (2013).
20. A. I. Hernandez-Serrano, E. Castro-Camus, and D. Lopez-Mago, "q-plate for the generation of terahertz cylindrical vector beams fabricated by 3D printing," *J. Infrared Millimeter Terahertz Waves* **38**, 938–944 (2017).
21. S. J. Ge et al., "Terahertz vortex beam generator based on a photo-patterned large birefringence liquid crystal," *Opt. Express* **25**(11), 12349–12356 (2017).
22. Z. W. Xie et al., "Spatial terahertz modulator," *Sci. Rep.* **3**, 3347 (2013).
23. S. Janne et al., "Holograms for shaping radio-wave fields," *J. Opt.* **4**(5), S161–S167 (2002).
24. V. C. Chen et al., "Micro-Doppler effect in radar-phenomenon, model and simulation study," *IEEE Trans. Aerosp. Electron. Syst.* **42**(1), 2–21 (2006).
25. V. C. Chen, "Micro-Doppler effect of micro-motion dynamics: a review," *Proc. SPIE* **5102**, 240–249 (2003).
26. V. C. Chen and F. Y. Li, "Analysis of micro-Doppler signatures," *IEE Proc. Radar Sonar Navig.* **150**(4), 271–276 (2003).

27. V. C. Chen and I. Ebrary, *The Micro-Doppler Effect in Radar*, 1st ed., Artech House, Boston, Massachusetts (2011).
28. P. A. George et al., "Integrated waveguide-coupled terahertz microcavity resonators," *Appl. Phys. Lett.* **91**(19), 191122 (2007).
29. Z. W. Wang et al., "On-chip single-mode high-Q terahertz whispering gallery mode resonator," *Opt. Lett.* **44**(11), 2835–2838 (2019).
30. J. Y. Xie et al., "Terahertz integrated device: high-Q silicon dielectric resonators," *Opt. Mater. Express* **8**(1), 50–58 (2018).
31. J. Y. Xie et al., "Terahertz-frequency temporal differentiator enabled by a high-Q resonator," *Opt. Express* **28**(6), 7898–7905 (2020).
32. X. L. Cai et al., "Integrated compact optical vortex beam emitters," *Science* **338**(6105), 363–366 (2012).
33. Z. K. Shao et al., "Spin-orbit interaction of light induced by transverse spin angular momentum engineering," *Nat. Commun.* **9**(1), 926 (2018).
34. X. K. Wang et al., "Longitudinal field characterization of converging terahertz vortices with linear and circular polarizations," *Opt. Express* **24**(7), 7178–7190 (2016).
35. G. B. Wu et al., "Orbital angular momentum (OAM) mode-reconfigurable discrete dielectric lens operating at 300 GHz," *IEEE Trans. Terahertz Sci. Technol.* **10**(5), 480–489 (2020).
36. R. Imai et al., "Generation of broadband terahertz vortex beams," *Opt. Lett.* **39**(13), 3714–3717 (2014).
37. B. A. Knyazev et al., "Generation of terahertz surface plasmon polaritons using nondiffractive Bessel beams with orbital angular momentum," *Phys. Rev. Lett.* **115**(16), 163901 (2015).
38. V. Boris et al., "Fabrication and characterization of diffractive phase plates for forming high-power terahertz vortex beams using free electron laser radiation," *Opt. Quantum Electron.* **48**, 223 (2016).
39. S. J. Ge et al., "Generating, separating and polarizing terahertz vortex beams via liquid crystals with gradient-rotation directors," *Crystals* **7**(10), 314 (2017).
40. P. Jan et al., "Chiral nanophotonic waveguide interface based on spin-orbit interaction of light," *Science* **346**(6205), 67–71 (2014).
41. M. Born and E. Wolf, Eds., *Principles of Optics*, Pergamon, Oxford (1980).
42. V. G. Farafonov and V. B. Il'm, "Rayleigh approximation for light scattering at parallelepipeds," *J. Opt. Technol.* **81**(7), 375–381 (2014).

Jingya Xie received her BS degree in electronic engineering from Xiamen University in 2009, and her MS and PhD degrees from Shanghai Jiao Tong University, in 2012 and 2015, respectively. She is currently an associate professor in Terahertz Technology Innovation Research Institute, and Shanghai Key Laboratory of Modern Optical System, University of Shanghai for Science and Technology. Her main research interests include photonic devices and their applications in terahertz field.

Linjie Zhou received his PhD from the Hong Kong University of Science and Technology, Hong Kong, China, in 2007. From 2007 to 2009, he was a postdoctoral researcher with the University of California, Davis, Davis, California, USA. He is currently a distinguished professor in the State Key Laboratory of Advanced Optical Communication Systems and Networks, Shanghai Jiao Tong University, Shanghai, China. His research interests include silicon photonics and photonic integration.

Yiming Zhu received his PhD from the University of Tokyo, Tokyo, Japan, in 2008. He is a "Youth Science and Technology Innovation Leader" and a "Young Yangtze Professor" with the University of Shanghai for Science and Technology, Shanghai, China, and currently serves as the vice director of the Shanghai Key Laboratory of Modern Optical System. His research interests include terahertz technologies and applications, including terahertz devices, terahertz spectroscopy, imaging systems, and terahertz bioapplications.

Biographies of the other authors are not available.